Structural Engineering and Mechanics, Vol. 9, No. 1 (2000) 69-88
DOI: http://dx.doi.org/10.12989/sem.2000.9.1.069

A model to analyze a buried structure response to surface dynamic loading

A.N. Dancygier† and Y.S. Karinski‡

Department of Civil Engineering, National Building Research Institute, Technion-Israel Institute of Technology, Haifa 32000, Israel

Abstract. A relatively simple model of a buried structure response to a surface loading that can simulate a possible opening and closure of a gap between the soil and the structure is presented. Analysis of the response of small and medium scale buried roof slabs under surface impulsive loading shows that the model's predictions are in fairly good agreement with the experimental results. Application of the model to a study case shows the relative influence of system parameters such as, the depth of burial, the arching coefficient, and the roof thickness, on the interface pressure and on the roof displacement. This model demonstrates the effect of a gap between the structure and the soil. The relative importance of including a gap opening and closure in the analysis is examined by the application of the model to a study case. This study results show that the deeper the depth of burial, the longer the gap duration, and the shorter the duration of the initial interface impact, while the higher the soil's shear resistance, the higher the gap duration, and the shorter the initial interface impact duration.

Key words: arching; buried structures; dynamic arching; gap; impact; soil-structure interaction.

1. Introduction

Analysis of the response of a buried structure to surface loading requires knowledge of the external surface loading, the way it is transmitted through the soil-backfill media, and how it interacts with the structure at the soil-structure boundary. For an external dynamic loading, most of the experimental and analytical studies focused on the response at the soil-structure boundary. For example, Getchell *et al.* (1984) conducted a series of tests of full scale buried structures that were subjected to external explosive excitation, which showed an interface loading that was different than that of the free field. Weidlinger *et al.* (1988) and Drake *et al.* (1989) proposed a Single Degree Of Freedom (SDOF) system model to simulate the effect of wave propagation at the soil-structure boundary. Their model accounts for the effect of the soil mechanical impedance, for the soil and the structure particle velocities, and for the free field loading, on the total interface pressure that is loading the structure. It allows de-coupling of the soil-structure system, and therefore, a separate analysis of the structure response. This model is usually applied under the assumption that an incident, uniformly distributed pressure wave, $p(t)$, propagates from the soil surface into the soil media. At the soil-structure interface, the structure response induces reflected and transmitted stress waves that depend on the structure velocity and on the incident wave. The structure's roof mass and

† Senior Lecturer
‡ Researcher

stiffness and the soil's mechanical impedance are presented in the SDOF model by adequate transformation factors, which are also used for an SDOF representation of the incident pressure, in order to form the structure's roof equation of motion. This model, which has been extensively used to analyze the response of a buried structure to dynamic loading (e.g., Chen *et al.* 1996), can also predict the time of a gap opening between the structure and the soil. However, being a SDOF model which de-couples the soil response from that of the structure, it cannot predict the gap closure time, nor can it analyze the response of the system after the gap closes. In some cases this analysis is sufficient to describe the main part of the structure response, which is the response to the initial interface impulse. However, when the gap opening duration is relatively short, or when the structure sustains the initial interface impulse, the response of the structure after the gap closes (or due to a process of multiple gap openings and closures) should be analyzed. In these cases, it is important to evaluate whether the gap remains open long enough to enable damping of further loading, or if the gap opening duration is so short that further loading of the structure will cause significant damage. Weidlinger and Hinman (1990) analyzed the characteristics of a soil-structure cavitation that develops under external dynamic excitation and its effects on the structure response. Their analysis used one-dimensional linear plane wave approximations and lumped mass models. That analysis used a pre-defined incident pressure wave at the soil-structure interface, which together with the soil's one-dimensional mechanical impedance represented the wave propagation phenomena in the soil medium above the structure.

A model of a buried structure subjected to surface impulse loading was proposed by the authors in a previous paper (Dancygier and Karinski 1999). The model (Fig. 1) delineates phenomena that relate both to wave propagation and to the effect of the soil shear resistance on the response. These phenomena consider, respectively, the relative particle *velocities* at the soil-structure interface, and the relative *displacements* in the soil media above and near the structure, as observed mostly under static loading conditions (e.g., Terzaghi 1943, Newmark 1964). However that model simulated the response only as long as no gap develops between the soil and the structure. This paper describes a

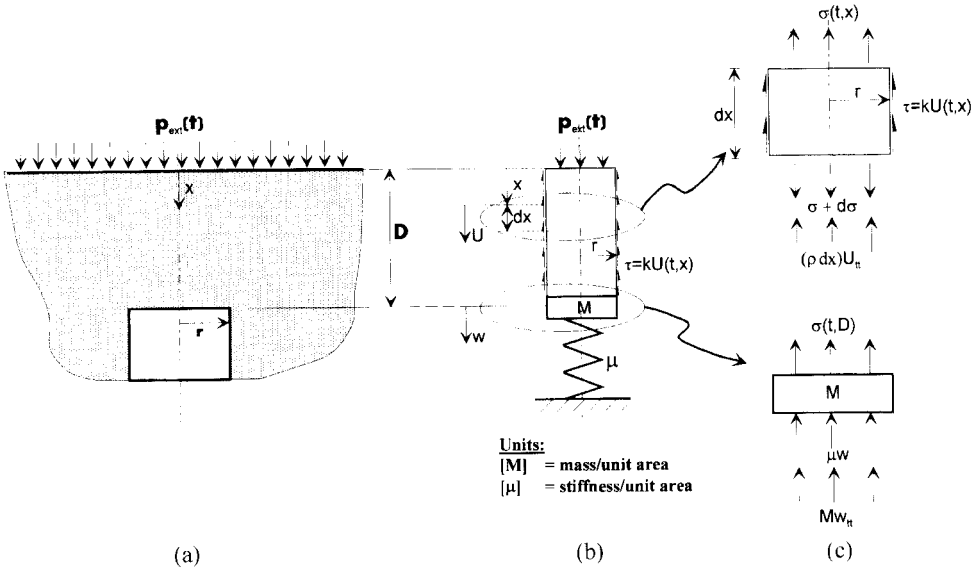

Fig. 1 Model of the soil-structure system

further development of the model, which includes simulation of the gap opening and closure, and shows the importance of considering this part of the response in the analysis of buried structures.

2. The model

The model is of an axisymmetric system and is described in Fig. 1b. It consists of a radial soil column attached at its bottom to a Single Degree Of Freedom (SDOF) mass (M) on spring (μ) system, representing the structure. The model assumes a linear elastic behavior for the soil and the structure (strains are assumed small). The surface loading is either uniformly distributed over a large area (relative to that of the structure roof), or assumed to generate a plane pressure wave into the soil (an assumption that is used also in other models, e.g., Drake *et al.* 1989, Weidlinger *et al.* 1988) in Fig. 1a. Material and geometric nonlinearities and radiation damping effects are not considered here. Damping effects may be important when the loading is acting on a relatively small area, or for relatively deep structures. These effects become negligible at relatively shallow depth of burial, or when the pressure wave front is relatively wide (e.g., as in the FOAM HEST experiments, Getchell *et al.* 1984). Nonlinearities and damping may be included in a further development of this model, which nevertheless in its current form agrees well with experimental results and shows the major trends and characteristics of the behavior (Dancygier and Karinski 1999, and also as shown later in the text).

Models of arching under static loading employed many times an analysis of a vertical shear failure surface that represented the somewhat curved, experimentally observed failure surface in the soil backfill. This approach simplifies the analysis and reduces it to a study of a soil column with a span that is similar to that of the buried structure (e.g., Terzaghi 1943, Allgood 1972, Murtha 1973). Similarly, in the current model, the soil column's radius, r, is equal to the radius of the structure, and its height, D, is equal to the soil backfill depth. The influence of soil arching, which is caused by the relative vertical *displacements* in the soil, above the roof mid-span and above its supports, on the soil-structure contact pressure, is included in the model by a friction traction, $\tau(t, x)$, which acts on the perimeter of the soil column, and depends on the vertical displacement, $U(t, x)$, Fig. 1b. For simplicity, the relation between $\tau(t, x)$ and $U(t, x)$ was assumed linear,

$$\tau(t, x) = k \cdot U(t, x) \tag{1}$$

where k is a constant, '*arching coefficient*', which depends on the soil properties, and represents its shear stiffness. In most cases the structure stiffness (represented in the current model by μ) is larger than the soil shear stiffness. The following analysis is performed for these cases, with a further assumption that the difference between μ and k is large enough to maintain the following condition, which is also necessary to obtain a mathematical solution in the form of a Fourier series (see below):

$$\frac{\mu}{M} > \frac{2k}{\rho r} \tag{2}$$

where M is the SDOF mass per unit area, μ is the SDOF spring stiffness per unit area, and ρ is the soil mass density.

The deflections of the SDOF mass, $W(t)$ and of the soil column bottom ($x=D$), $U(t, D)$, are identical as long as the contact stress between the soil and the structure, $\sigma(t, D)$, is compressive, that is, as long as, $\sigma(t, D) = E \cdot U_x(t, D) \leq 0$, where E is the soil Young's modulus, and $U_x = \partial U(t, x)/$

∂x. A positive contact stress, $\sigma(t, D)$, marks a gap opening, which sets the soil-structure contact pressure to zero, and an independent motion of the structure and of the soil. This state continues until the gap closes when there is another contact between the soil and the structure, which occurs on condition that $W(t) = U(t, D)$ (no overlapping).

2.1. Mathematical formulation and solution

Mathematically, the model for a state of a closed gap (Fig. 1b, c) is described by the one dimensional wave propagation equation:

$$\rho\ddot{U} - EU_{xx} + \frac{2}{r}kU = 0 \tag{3}$$

with the initial conditions (at t=0 or after each closure of the gap):

$$U(t_0, x) = U_p(t_0, x)$$
$$\dot{U}(t_0, x) = \begin{cases} \dot{U}_p(t_0, x); & 0 \le x < D \\ \dot{W}_p(t_0) \quad ; & x = D \end{cases} \tag{4}$$

where t_0 is the last gap closure time, U_p, $\dot{U}_p$, are the soil displacement and velocity of the "previous state" at $t=t_0$ ($U_p(t_0, D)=W_p(t_0)$), and W_p, $\dot{W}_p$, are the mass (structure) displacement and velocity (at the same time, t_0). When the soil-structure gap is opened or closed, the conditions prior to the gap closure or opening are defined as a "previous state".

The boundary conditions are:

$$U_x(t, 0) = p(t)/E \tag{5}$$

$$\ddot{U}(t, D) + c_1^2 U_x(t, D) + \tilde{\mu} U(t, D) = 0 \tag{6}$$

where $c_1^2 = E/M$, $\tilde{\mu} = \mu/M$, $\ddot{U} = \partial^2 U/\partial t^2$, and $U_x = \partial U/\partial x$. The first boundary condition, Eq. (5), expresses the normal stress at the soil surface, and the second condition, Eq. (6), is the SDOF mass equation of motion, Figs. 1b and c.

For the open gap state, the soil motion is described by Eq. (3) with the initial conditions Eq. (4) (where $t_0=t_G$ is the gap opening time, $\dot{W}_p=\dot{U}_p(D)$), and with the following boundary conditions:

$$U_x(t, 0) = p(t)/E \tag{7}$$
$$U_x(t, D) = 0$$

The equation of motion and initial conditions of the mass, M, are given, respectively, by Eqs. (8) and (9):

$$\ddot{W}(t) + \tilde{\mu} W(t) = 0 \tag{8}$$

$$W(t_G) = U_p(t_G, D)$$
$$\dot{W}(t_G) = \dot{U}_p(t_G, D) \tag{9}$$

The gap opening and closure conditions are as follows:
A gap is opened at:

$$EU_x(t, D)=0 \tag{10}$$

An open gap is closed at: $U(t, D)=W(t)$

The solution of Eqs. (8) and (9) is given by:

$$W(t)=U_p(t_G, D)\ \cos[\sqrt{\tilde{\mu}}(t-t_G)]+\frac{\dot{U}_p(t_G, D)}{\sqrt{\tilde{\mu}}}\sin[\sqrt{\tilde{\mu}}(t-t_G)] \tag{11}$$

The following substitution is carried out in order to obtain homogenous boundary conditions for the soil column:

$$\tilde{U}(t, x)=U(t, x)+\frac{p(t)}{E}\frac{(D-x)^2}{2D} \tag{12}$$

Hence, the wave equation, Eq. (3), and the initial and boundary conditions, Eq. (4) and Eqs. (5), (6), and (7), will take the form:

$$\ddot{\tilde{U}}-c^2\tilde{U}_{xx}+\tilde{k}\tilde{U}=\varphi(t, x) \tag{13}$$

$$\tilde{U}(t_0, x)=f_0(x); \qquad \dot{\tilde{U}}(t_0, x)=f_1(x); \tag{14}$$

$$\tilde{U}_x(t, 0)=0; \quad \begin{cases} \ddot{\tilde{U}}(t, D)+c_1^2\tilde{U}_x(t, D)+\tilde{\mu}\tilde{U}(t, D)=0 & \text{for a closed gap} \\ \tilde{U}_x(t, D)=0 & \text{for an open gap} \end{cases} \tag{15}$$

where $c^2=E/\rho$, $\tilde{k}=2k/\rho r$, the gap opening time $t_0\equiv t_G$, and,

$$\varphi(t, x)=\frac{1}{2DE}[(\ddot{p}(t)+\tilde{k}p(t))(D-x)^2-2c^2p(t)] \tag{16}$$

$$f_0(x)=\frac{p(t_0)}{2DE}(D-x)^2+\tilde{U}_p(t_0, x); \qquad f_1(x)=\frac{\dot{p}(t_0)}{2DE}(D-x)^2+\begin{cases} \dot{\tilde{U}}_p(t_0, x); & 0\le x<D \\ \dot{W}_p(t_0); & x=D \end{cases} \tag{17}$$

The solution is sought by applying the Fourier method, thus:

$$\tilde{U}(t, x)=\sum_{n=0}^{\infty}T_n(t)X_n(x) \tag{18}$$

Subject to the condition that $\tilde{k}\le\tilde{\mu}$ (see Eq. 2), the eigenfunctions $X_n(x)$ are solutions of the following boundary problem:

$$X_n''-\vartheta_n^2X_n=0 \tag{19}$$

– for a closed gap: $$X_n'(0)=0; \quad c_1^2X_n'(D)+(\tilde{\mu}+\lambda_n)X(D)=0 \tag{20}$$

– for an open gap: $$X_n'(0)=0; \quad X_n'(D)=0 \tag{21}$$

where,

$$\lambda_n=-(\tilde{k}+c^2\vartheta_n^2) \tag{22}$$

which satisfies $-c^2\vartheta_n^2=\tilde{k}+\lambda_n<0$ in order to yield a non-trivial solution. The boundary conditions, Eq. (20), yield the eigenvalue, ϑ_n, that satisfies the following equation:

$$tg(\vartheta_n D)=\frac{\tilde{\mu}-\tilde{k}}{c_1^2\vartheta_n}-\frac{M\vartheta_n}{\rho} \tag{23}$$

and the solution of Eq. (19) is given by the eigenfunctions: $X_n(x)=\cos(\vartheta_n x)$. Note that the structure properties, which are represented in this model by a SDOF system, are included in the modes of the overall, continuous, soil-structure model through the parameters ϑ_n.

Orthogonality conditions for the eigenfunction system are as follows:

$$\int_0^D X_n(x)X_m(x)dx+\frac{M}{\rho}X_n(D)X_m(D)=0;\quad (n\neq m) \tag{24}$$

and the norm of the eigenfunction, X_n, has the form:

$$\|X_n\|^2=\int_0^D X_n^2(x)dx+\frac{M}{\rho}X_n^2(D)=\frac{D}{2}+\frac{1}{2}\left(\frac{\tilde{\mu}-\tilde{k}}{c_1^2\vartheta_n^2}+\frac{M}{\rho}\right)\left[1+\left(\frac{\tilde{\mu}-\tilde{k}}{c_1^2\vartheta_n^2}-\frac{M\vartheta_n}{\rho}\right)^2\right]^{-1} \tag{25}$$

For the boundary conditions, Eq. (21), the classical solution is obtained in the following form:

$$X_n(x)=\cos\left(\frac{\pi n}{D}x\right);\qquad \vartheta_n=\frac{\pi n}{D} \tag{26}$$

$$\int_0^D X_n(x)X_m(x)dx=0;\quad (n\neq m);\qquad \|X_n\|^2=\begin{cases} D/2; & n\neq 0\\ D; & n\neq 0\end{cases} \tag{27}$$

Expansion of the functions given in Eqs. (16) and (17) in terms of $X_n(x)$, subject to the orthogonality conditions, Eqs. (24) and (27), yields:

$$\varphi(t,x)=\sum_{n=0}^{\infty}\varphi_n(t)X_n(x);\quad f_j(x)=\sum_{n=0}^{\infty}f_{jn}X_n(x);\quad j=0,1 \tag{28}$$

where, for a closed gap:

$$\varphi_n(t)=\frac{\ddot{p}(t)+\tilde{k}p(t)}{ED}\,\frac{D\vartheta_n-\sin(D\vartheta_n)}{\vartheta_n^3\|X_n\|^2}+\frac{c^2}{ED}p(t)\frac{\sin(D\vartheta_n)}{\vartheta_n\|X_n\|^2} \tag{29}$$

$$f_{0n}=\frac{p(t_0)}{ED}\cdot\frac{D\vartheta_n-\sin(D\vartheta_n)}{\vartheta_n^3\|X_n\|^2}+\frac{1}{\|X_n\|^2}\left[\frac{M}{\rho}W_p(t_0)\cos(\vartheta_n D)+\int_0^D\tilde{U}_p(t_0,x)\cos(\vartheta_n x)dx\right] \tag{30}$$

and for an open gap:

$$\varphi_n(t)=\begin{cases}\dfrac{\ddot{p}(t)+\tilde{k}p(t)}{2ED}\left(\dfrac{2D}{\pi n}\right)^2 & ;\quad n\neq 0\\[2ex] \dfrac{\ddot{p}(t)+\tilde{k}p(t)}{2E}\dfrac{D}{3}-\dfrac{c^2}{ED}p(t); & n=0\end{cases} \tag{31}$$

$$f_{0n}=\begin{cases}\dfrac{p(t_0)}{E}\cdot\dfrac{2D}{(\pi n)^2}+\dfrac{2}{D}\int\limits_0^D\tilde{U}_p(t_0,x)\cos\left(\dfrac{\pi n}{D}x\right)dx; & n\neq 0\\[2ex] \dfrac{p(t_0)}{6E}\cdot D+\dfrac{1}{D}\int\limits_0^D\tilde{U}_p(t_0,x)\cos\left(\dfrac{\pi n}{D}x\right)dx; & n=0\end{cases} \tag{32}$$

For both open and closed gap $f_{1n}=\partial f_{0n}/\partial t_0$. Substituting the Fourier transformation of the solution for the "previous" state at $t=t_0$, $\tilde{U}_p(t_0,x)$, in the integrals in Eqs. (30) and (32) yields,

– for a closed gap:

$$f_{0n}=\frac{1}{\|X_n\|^2}\left[\frac{p(t_0)}{ED}\cdot\frac{D\vartheta_n-\sin(D\vartheta_n)}{\vartheta_n^3}+\frac{M}{\rho}W_p(t_0)\cos(\vartheta_n D)+\vartheta_n\sin(\vartheta_n D)\sum_{m=0}^{\infty}T_{m,p}(t_0)\frac{(-1)^m}{\vartheta_n^2-(\pi m/D)^2}\right] \tag{33}$$

– for an open gap:

$$f_{0n}=\begin{cases}\dfrac{p(t_o)}{E}\cdot\dfrac{2D}{(\pi n)^2}+(-1)^n\dfrac{2}{D}\sum\limits_{m=0}^{\infty}T_{m,p}(t_0)\dfrac{\sin(\vartheta_m D)}{\vartheta_m^2-(\pi n/D)^2}; & n\neq 0\\[2ex] \dfrac{p(t_o)}{6E}\cdot D+\dfrac{1}{D}\sum\limits_{m=0}^{\infty}T_{m,p}(t_0)\dfrac{\sin(\vartheta_m D)}{\vartheta_m}; & n=0\end{cases} \tag{34}$$

where the terms $T_{m,p}(t_0)$ are the time functions in the Fourier series (see Eq. 18) of the "previous" state at $t=t_0$ ($T_{m,p}(0)=0$ for any m). Hence, the functions $T_n(t)$ are obtained from the following equation and initial conditions:

$$\ddot{T}_n(t)+\tilde{\lambda}_n^2T(t)=\varphi_n(t) \tag{35}$$

$$T_n(0)=f_{0n};\quad \dot{T}_n(0)=f_{1n} \tag{36}$$

where $\tilde{\lambda}_n^2=-\lambda_n$ (see Eq. 22).

The solution, Eqs. (35) and (36), yields:

$$T_n(t)=f_{0n}\cos(\tilde{\lambda}_n t)+\frac{f_{1n}}{\tilde{\lambda}_n}\sin(\tilde{\lambda}_n t)+\frac{1}{\tilde{\lambda}_n}\int_0^t\varphi_n(\tau)\sin[\tilde{\lambda}_n(t-\tau)]d\tau \tag{37}$$

and the solution to the model that describes the motion of the soil column is given by:

$$U(t,x)=-\frac{p(t)}{2ED}(D-x)^2+\sum_{n=0}^{\infty}T_n(t)\cos(\vartheta_n,x) \tag{38}$$

Expressions (11) and (38) are an analytical, closed form solution of the model, for both open and

closed gap conditions. This solution does not require any numerical integration of the differential equations, but only the calculation of the Fourier series, Eq. (38). The number of the eigenfunctions adopted in the calculation is determined numerically by a convergence criterion of the Fourier series. In all the following examples fifteen or less eigenfunctions were sufficient.

2.2. Application of the model

The above model may be applied to various roof shapes if r_{eq} substitutes r in Eq. (3). The term r_{eq} is an equivalent radius that depends on the roof shape. Because the model is one-dimensional, r_{eq} ensures only that dynamic equilibrium is satisfied according to Eq. (3). For example, r_{eq} of a circular roof is its radius r, and for a $B \times L$ rectangular roof,

$$r_{eq} = \frac{L \times B}{(L + B)} \tag{39}$$

and the SDOF transformation factors of the roof stiffness and mass are obtained according to the roof thickness, elastic properties, and boundary conditions.

Possible ways to set the arching coefficient k, Eq. (1), are described by Dancygier and Karinski (1999), where it is shown that k would vary, depending on the soil properties, from zero (no arching effect) to approximately $E/3r$ ($0.3431E/r$, maximal arching effect). When static data are available, such as measurements from static tests of the external pressure, p_{ext}, and of the interface pressure, k may be obtained by applying the current model under static loading conditions (Fig. 1b and c with the inertia terms, U_{tt} and W_{tt}, set to zero). For example, measurements of the external and of the contact pressures were taken in a static test of a one way, 24×24 inches (609.6×609.6 mm), fixed, concrete roof slab (Kiger *et al.* 1984, Kiger 1988). From these measurements it can be shown that the arching coefficient, k, of the 'Reid-Bedford model sand' that was used in this test, was equal to 0.2104 N/m^3, which is also $0.62(E/3r_{eq})$ (Dancygier and Karinski 1999).

3. Comparison with experimental results

The proposed model was applied to small scale tests of buried, circular, micro-concrete roof slabs (Keer *et al.* 1991), and to medium scale tests of buried, one way, fully fixed, reinforced concrete roof slabs (Kiger *et al.* 1984). In the simulation of the small scale tests one test was modeled with an assumed value of the arching coefficient, k, (between 0 and $E/3r$), and another test was simulated with the same coefficient. In the medium scale tests (Kiger *et al.* 1984) k was evaluated from the reported interface pressure that was measured under an external, static pressure, as explained above.

3.1. Small scale experiments

Small-scale experiments were conducted with circular roof slabs that were made of micro-concrete (a gypsum-sand-water mixture, Cunningham *et al.* 1986), and were buried in 20-30 Ottawa sand (Keer *et al.* 1991). A mechanical impact of a dropped steel ball on a circular aluminum target plate that rested on the soil surface produced the external load. Two tests were simulated by the current model: a simply supported roof slab under 2.5 inches (63.5 mm) of soil backfill, and a clamped (not fully fixed, but with a certain curvature restraint at the perimeter) roof slab under 3 inches (76.2 mm) of soil

backfill. The small-scale test parameters are given in Table 1, and the external pressure in the tests that were simulated is shown in Fig. 2. The simulation was done in two stages: first, the model was applied to a test of a simply supported roof slab, with properties that were selected in order to obtain a good agreement of the model with the test. These parameters were as follows: an arching coefficient, k, equal to 0.4(E/3r), a micro-concrete Poisson's ratio of 0.3 and Young's modulus of $1.0 \cdot 10^{10}$ Pa. This modulus of elasticity is low, relative to the reported 5000-psi (34.5 MPa) micro-concrete compressive strength (e.g., according to the ACI code, ACI 1988). However, a relatively low modulus of elasticity of the micro-concrete was indeed reported (Keer *et al.* 1991).

In the second stage a clamped roof slab was simulated by the model with the same values of k, of the micro-concrete Poisson's ratio, and a similar Young's modulus corrected according to the micro-concrete higher compressive strength in this test. The micro-concrete compressive strength was 5000 psi (34.5 MPa) and 6000 psi (41.4 MPa) in the tests with the simply supported and the clamped roof slabs, respectively, therefore the 1.0×10^{10} Pa modulus of elasticity was increased by a ratio of $\sqrt{6000/5000}$. The clamping device in this test supplied only partial clamping to the slab, hence, its response was of a partially clamped circular roof. Therefore, in order to examine the upper and lower bounds of the structure response, the model was applied with the fixed and the simply supported boundary conditions for the circular roof (i.e., different SDOF transformation factors for each boundary condition, see K_l and K_m values in Table 1 and Figs. 5, 6).

Table 1 Input data of the simulations

			Small scale tests			Medium scale test	Numerical example
			Simply supported roof slab	Clamped roof slab		Fixed roof slab	Fixed roof slab
			circular	circular	circular	rectangular	circular
Variable		Description	simply supported model	simply supported model	fixed roof model	fixed roof model	fixed roof model
S	r	mass density (Kg/m^3)	1711	1711		1636	1760
O	c	longitudinal wave speed (m/sec)	353	293		435	250
I	D	depth of burial (mm)	63.5	76.2		304.8	varies
L	$k/(E_{soil}/3r)$	normalized arching coefficient	0.4*	0.5796*		0.62	varies
S	K_l	SDOF stiffness transformation factor	0.4591	0.4591	.3333	.5333	.3333
T	K_m	SDOF mass transformation factor	0.2945	0.2945	.2000	.4063	.2000
R	E_s	Young's modulus (Pa)	1.0×10^{10}	1.1×10^{10}		3.1×10^{10}	3.0×10^{10}
U	ν	Poisson's ratio	0.3	0.3		0.1	0.15
C	h	roof thickness (mm)	10.9	11.2		73.7	200, 250, 400
T	r	roof radius (mm)	63.5	63.5		304.8**	4000
U	μ	equivalent stiffness (N/m^3)	0.526×10^9	0.627×10^9	1.857×10^9	1.553×10^9	1.705×10^6, 3.33×10^6, 13.64×10^6
R	ρ_s	mass density (Kg/m^3)	2085	2085		2400	2400
E	M	equivalent mass (Kg/m^2)	6.69	6.88	4.67	71.84	96, 120, 192

* In the simulations of both small scale tests the arching coefficient, k, was equal to 0.4471×10^9 N/m^3

** Equivalent radius of a rectangular, one way roof (L=B=609.6 mm)

Notes: 1. The soil Young's modulus, E_{soil}, is equal to Pc^2.

2. Poisson ratios were assumed for concrete and for micro-concrete.

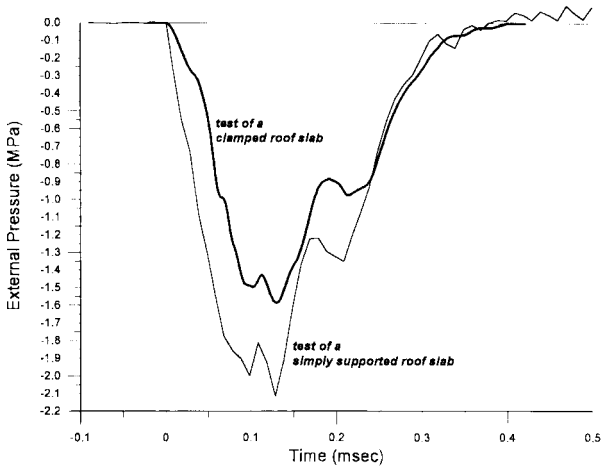

Fig. 2 External (surface) pressure in the small scale tests

The interface pressure and the mid-roof displacement that were measured in the tests and that are predicted by the model, are shown in Figs. 3-6. These figures show that the model's simulations are in fairly good agreement with the experimental measurements. The model captures the initial peak of the interface pressure, its duration, and the development of a gap between the soil and the structure. The simply supported model was calibrated in order to give a good agreement with the experimental results. It is interesting to observe that even in this case, in addition to the initial peak of the interface pressure, the models prediction of the gap opening time and duration agrees well with the experimental result (Fig. 3).

The model differs from the experimental results when the gap closes and at a relatively later time of the response. The gap closure in the model is characterized by an abrupt increase of the interface pressure, which is typical of an impact between two colliding bodies. In the experiments, however, the gap closure is more gradual, because of the damping (which is not modeled) and due to the frequency of the data acquisition in the experiments. In fact, when the response was calculated in the model at larger time steps, the pressure increase at the gap closure became more moderate. Later in the response, a pressure wave is expected to be reflected from the soil surface at 0.54 msec and at 0.78 msec in the tests with the 2.5 inches (simply supported) and 3 inches (clamped) depth of burial, Figs. 3 and 5, respectively. This reflection is modeled in the current simulation, which does not include damping. However, a reflection from the soil surface did not show in the experimental measurements, where damping is expected to be very effective at this relatively late time of the response. This un-damped reflected wave causes the numerically simulated structure to oscillate. It is interesting to note though, that in spite of the difference between the theoretical and the experimental response after the reflected wave arrival time, the structure displacement oscillates close to, or around the experimentally measured displacement (Figs. 4 and 6).

3.2. A medium scale experiment

The medium scale experiment was of a fully fixed, one-way, rectangular, reinforced concrete roof slab, which was subjected to surface explosive loading (Kiger *et al.* 1984). The systems properties are given in Table 1, and the external pressure is shown in Fig. 7 (copied from Kiger *et al.* 1984). The

arching coefficient was obtained from static loading measurements, as cited above (section 2.2.). Fig. 8 shows the result of the simulation, together with the interface pressure that was measured 7 inches from the roof center (the mid-roof pressure gage was reported to be broken, and furthermore, this measurement better represents an average interface pressure acting over the roof). Since the roof slab in this test failed, it was clear that the structure displacement exceeded its elastic range. Nevertheless, this test was modeled, because the static tests showed that at a displacement of about 3-4 mm the roof slab yielded (see insert in Fig. 8), hence the model may be compared to the experimental result up to the point when the mid-roof slab reached this displacement. Fig. 8 shows that the current model captures well the initial peak interface pressure and duration. It ceases to match the experiment when the structure response exceeds the elastic range, while the model remains linear-elastic.

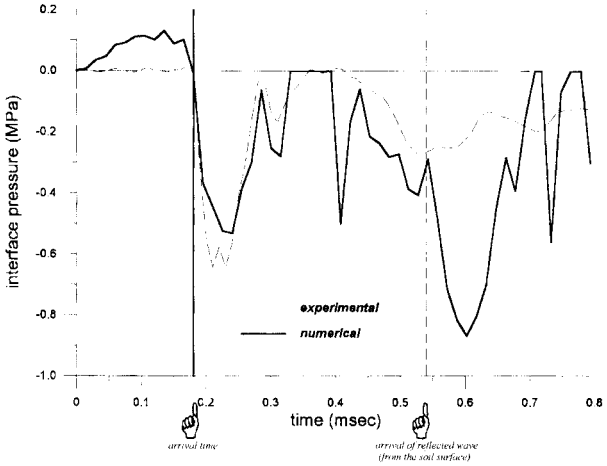

Fig. 3 Interface pressure at the plate center in a test of a simply supporte roof slab; h = 10.9 mm, D = 63.5 mm, $k = 0.4(E/3R) = 0.447\times10^9$ N/m^3

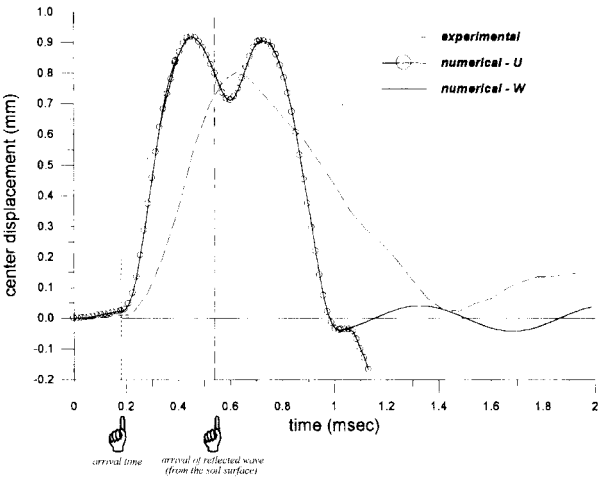

Fig. 4 Vertical displacement in a test of a simply supported roof slab; h = 10.9 mm, D = 63.5 mm, $k = 0.4(E/3R) = 0.447\times10^9$ N/m^3

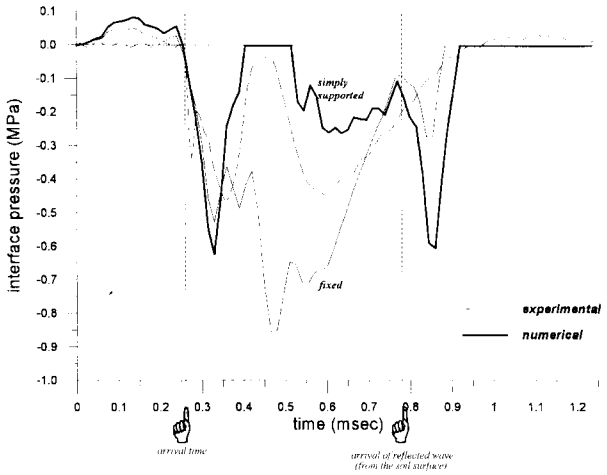

Fig. 5 Interface pressure at the plate center in a test of a clamped roof slab; $h = 11.2$ mm, $D = 76.2$ mm, $k = 0.58(E/3R) = 0.447\times10^9$ N/m^3

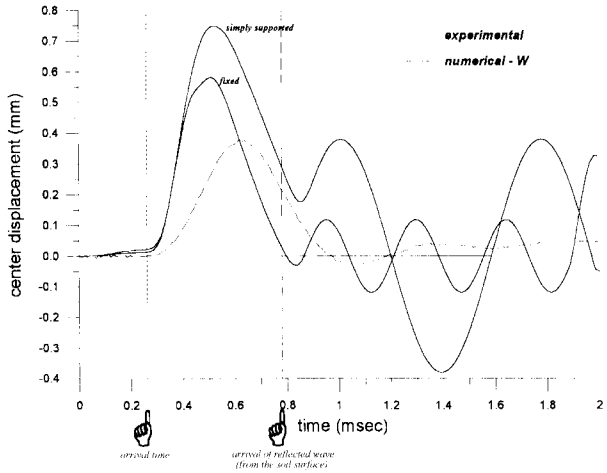

Fig. 6 Vertical displacement in a test of a clamped roof slab; $h = 11.2$ mm, $D = 76.2$ mm, $k = 0.58(E/3R) = 0.447\times10^9$ N/m^3

4. A numerical example

The effects of a problem's typical parameters on the loading and response of a buried structure are demonstrated in the following numerical example, by application of the model to a study case. Consider a circular, buried concrete structure, with a fixed, 4-m radius roof, subjected to a uniformly distributed external impact. The other properties of the soil backfill, and of the structure are given in Table 1. A Hanning's function for a monopeak, smooth-shaped curve was chosen for the loading time function of the external load, $p(t)$, in this example, thus:

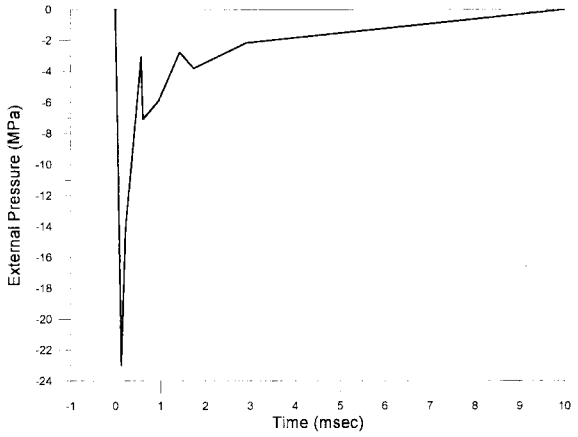

Fig. 7 External pressure in the medium scale test (Kiger *et al.* 1984)

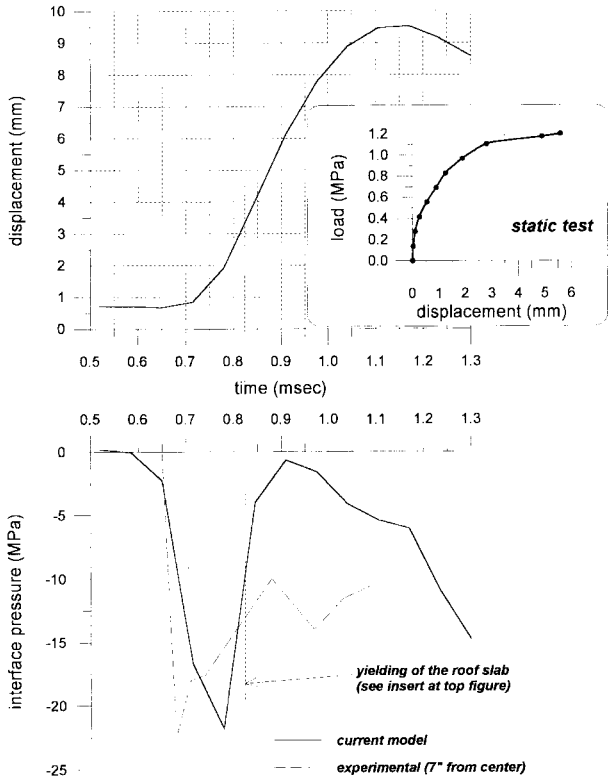

Fig. 8 Vertical displacement and interface pressure in the medium scale test (Kiger *et al.* 1984)

$$p(t)=\frac{p_0}{2}\begin{cases}1-\cos\left(\dfrac{2\pi t}{T_0}\right); & t\le T_0\\ 0 \quad ; & t>T_0\end{cases} \tag{40}$$

where the impact amplitude, p_0, is 1 MPa, and its duration, T_0, is 15 msec.

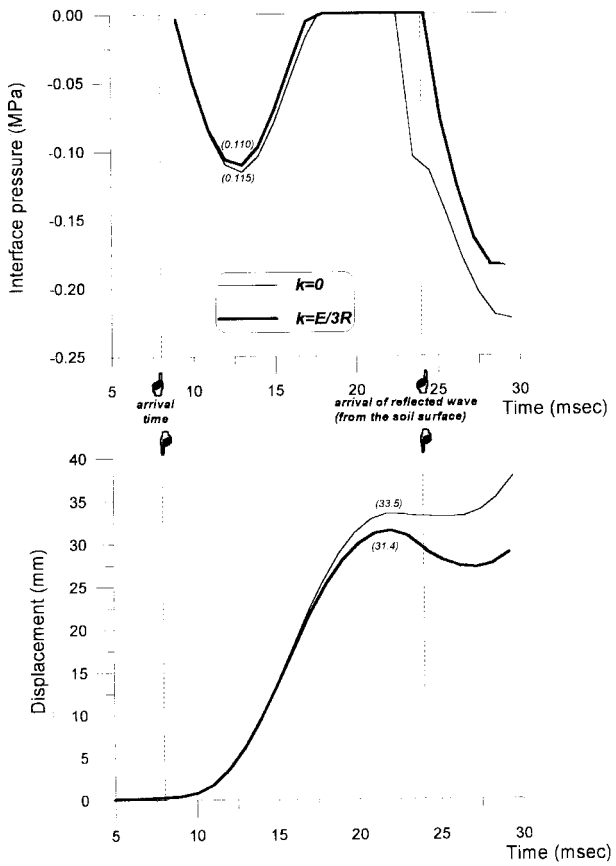

Fig. 9 Response of a circular buried structure; $D = 2$ m, $R = 4$ m, $h = 250$ mm

The solution of this example was obtained at $x=D$ (D is the depth of burial), with the above parameters (see also Table 1), with different values of the soil arching coefficient, k, and for different depths of burial. Figs. 9-11 show, respectively, the interface pressure and displacement history for depths of burial, $D=R/2$, R, and $2R$. Note that the analysis is considered within a time interval of three arrival times ($3\times D/c$, where c is the pressure wave propagation speed in the soil), when a pressure wave is expected to be reflected from the soil surface. It can be seen in the figures that when the arching coefficient is equal to $E/3R$ there is a reduction of the displacement and of the peak interface pressure as compared to a system without soil arching. The reductions are 6% and 4%, 10% and 5%, 18% and 8%, at $D = 2$, 4, and 8 m, in the peak displacement and interface pressure, respectively (Figs. 9, 10, and 11). These results show that when soil arching develops (with $k = E/3R$), the interface pressure reduces and so does the structure displacement, although the relative reduction of the interface pressure is smaller than that of the displacement. They also show that the deeper the soil backfill the stronger the influence of soil arching. An important part of this result is the longer gap duration, t_{GAP}, which is caused when soil arching is developed (compare the duration of the zero interfaces pressures at the top of Figs. 9-11). A longer gap not only prolongs the time during which the mid-structure is relieved of external load, but it also causes a reduction of the initial interface impulse. Note that if there is no soil arching ($k = 0$) different soil depths do not yield different interface pressure peaks nor

different response, because the model does not include dissipation of the external load.

The importance of the gap influence on the response is further demonstrated by comparing the response of a 250 mm and a 400 mm thick roof slabs, at a depth of 4 m, without soil arching ($k = 0$), under the external loading of the above example. The SDOF parameters of the 250-mm and 400-mm roof slabs are, respectively: μ=0.333 · 10^7 and 1.364 · 10^7 N/m^3, M=120 and 192 Kg/m^2, T_s=37.7 and 23.6 msec (T_s is the natural period of the structure's SDOF model). The dynamic amplification factors (DAF) for a sinusoidal impulse of 15 msec are 1.4 and 1.7 (Clough and Penzien 1975). Fig. 12 shows the response of these slabs, according to the current model. It shows that the initial peak interface pressure at the thicker roof slab is about twice as much as the peak interface pressure over the 250-mm roof slab (0.231 and 0.122 MPa, Fig 12). Therefore, the reduction in the peak roof displacement is obtained as follows:

$$W_{\max}=DAF\times\frac{p_{\max}}{\mu}\Rightarrow\frac{w_{h=400}}{w_{h=250}}=\frac{1.7}{1.4}\times\frac{0.23}{0.12}\times\frac{0.333\times10^7}{1.364\times10^7}\times100=57\% \tag{41}$$

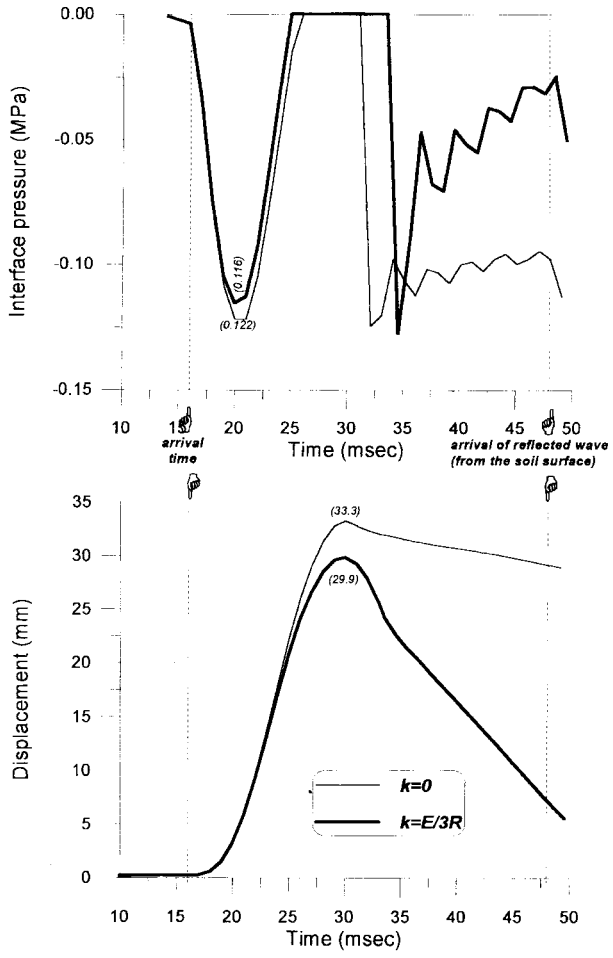

Fig. 10 Response of a circular buried structure; $D = 4$ m, $R = 4$ m, h =250 mm

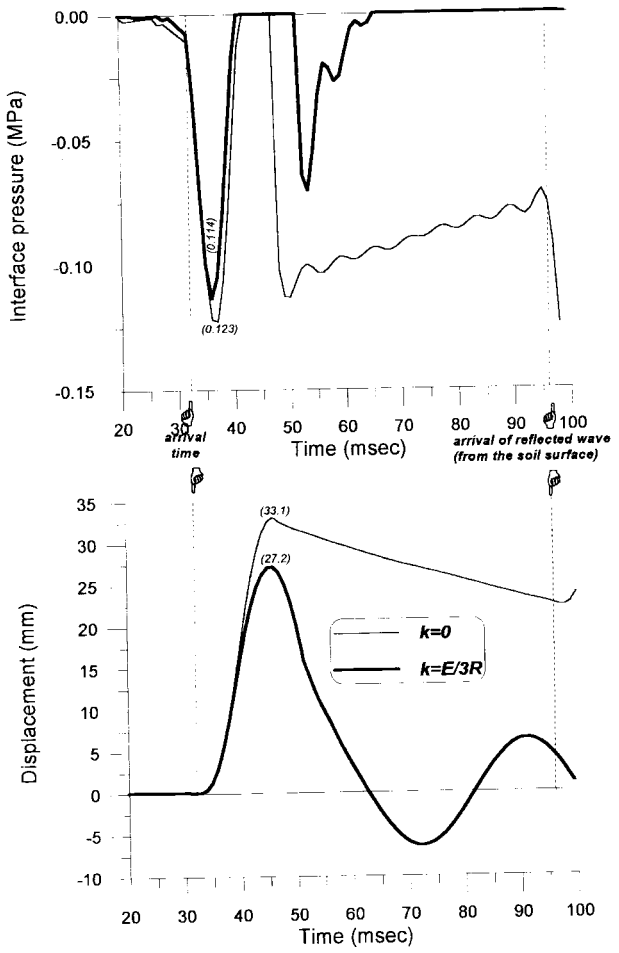

Fig. 11 Response of a circular buried structure; $D = 8$ m, $R = 4$, $h = 250$ m

where p_{max} is the peak interface pressure (top of Fig. 12). However, although according to this result it is expected that compared to the 250-mm roof slab, the peak displacement of the thicker roof slab would be reduced by 43%, it is reduced only by 14% (Fig. 12). This result demonstrates the effect of the gap opening (and of the gap opening duration) on the total response. It can be seen in Fig. 12 that the interface pressure over the 250-mm roof slab has not only a smaller peak, but it also has a shorter duration. That initial interface impulse is followed by the formation of a gap (zero interface pressure), which does not open over the thicker and stiffer roof slab.

The combined effect of the soil arching coefficient, k, and of the soil backfill depth, D, is shown in Fig. 13. It can be seen in the figure that the deeper the depth of burial the longer the gap duration (Fig. 13a), and the shorter the duration of the initial interface impact (Fig. 13b). It also shows the effect of soil arching on attenuating the loading on the structure: the higher the arching effect (the higher k) the higher the gap duration (Fig. 13a) and the shorter the initial interfaces impact duration (Fig. 13b). Furthermore, Fig. 13b also indicates the relative effects of

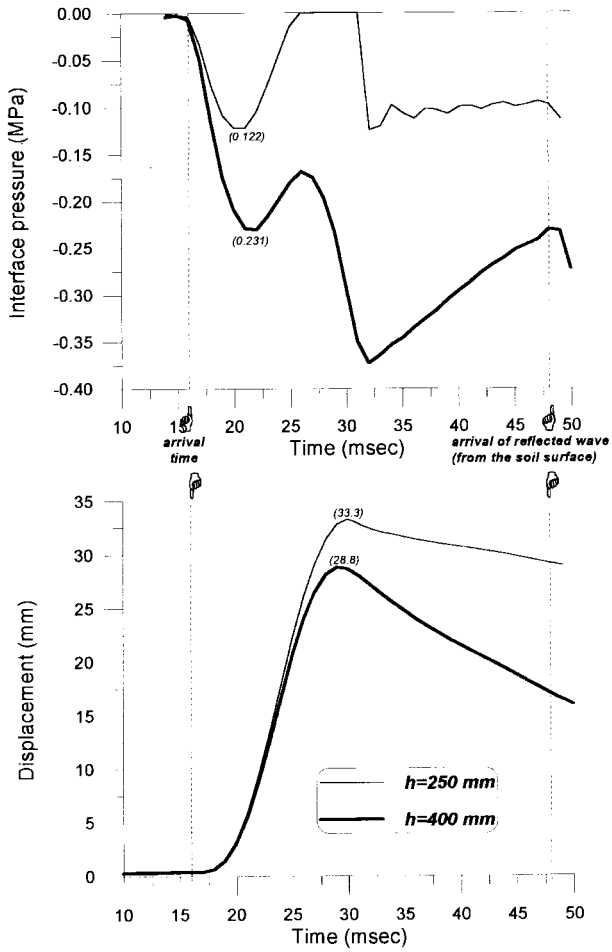

Fig. 12 Response of a circular buried structure; $D = 4$ m, $R = 4$ m, $k = 0$

wave propagation phenomenon and of soil arching on the interface loading: Without soil arching ($k = 0$) the interface loading is affected by phenomena that are related to wave propagation (e.g., the relative velocity of the soil-structure particles at the soil-structure interface). As the soil shear resistance (that affects the soil capability to develop arching) increases, the interface loading further decreases, as it is indicated here by a longer gap duration, and a shorter duration of the initial interface impact.

The gap closure is characterized by an abrupt increase of the interface pressure, which is typical of an impact between two colliding bodies (Figs. 10 and 11), as also observed in the small-scale simulations (see section 3.1).

5. Conclusions

A relatively simple model of a buried structure response to a surface loading that can also simulate a possible opening and closure of a gap between the soil and the structure, is presented.

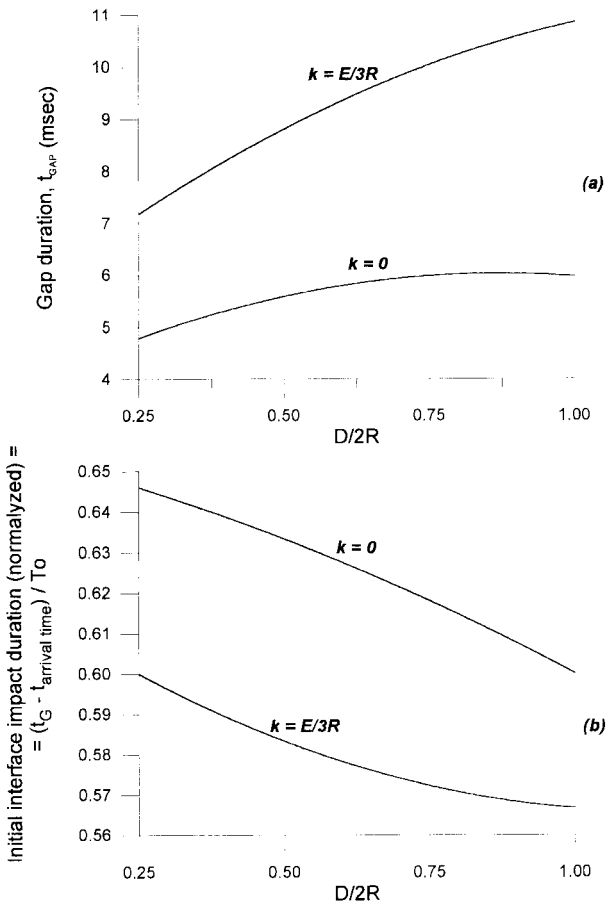

Fig. 13 Effect of depth of burial (D) and of the soil arching coefficient (k) on the gap duration (t_{GAP}) and on the initial interface impact duration ($T_0 = 15$ msec, $h = 250$ mm)

Analysis of the response of small and medium scale buried roof slabs under surface impulsive loading shows that the model's predictions are in fairly good agreement with the experimental results. The relative importance of including a gap opening and closure in the analysis is demonstrated by application of the model to a study case of a buried structure under external transient dynamic loading. The results show the relative influence of the depth of burial and arching coefficient, and of the roof thickness, on the interface pressure and on the roof displacement. The deeper the depth of burial the longer the gap duration, and the shorter the duration of the initial interface impact. In addition to the influence on the response of wave propagation phenomena, the current analysis shows that the higher the soil's shear resistance (the higher the 'static' arching effect) the higher the gap duration, and the shorter the initial interface impact duration. When there are conditions that cause a development of a gap between the soil and the structure, the structure is relieved of the interface pressure and its displacement is reduced.

Considering the simplicity of the model, it simulates well the overall trends and characteristics of a buried structure behavior under dynamic surface impact. Nonlinearities of the soil and of the structure and damping effects, as well as gravitational influence, may be included in a further development of

the model for problems of very deep structures or a surface loading that acts over a relatively small area.

Acknowledgements

Partial financial support for this work was provided by the Center for Scientist Absorption at the Ministry for Absorption of Aliah, Jerusalem.

References

Allgood, J.R. (1972), "Summary of soil-structure interaction", Technical Report R-771, AD-748581, NCEL, Port Hueneme, California, July.

American Concrete Institute (1995), *Building Code Requirements for Reinforced Concrete*, ACI 318-95, Detroit, Michigan, June.

Clough, R.W. and Penzien, J. (1975), *Dynamics of Structures*, McGraw-Hill Book Company, Singapore.

Chen, H.L. and Chen, S.E. (1996), "Dynamic responses of shallow-buried flexible plates subjected to impact loading", *Journal of Structural Engineering, ASCE*, **122**(1), January.

Cunningham, C.H., Townsend, F.C. and Fagundo, F.E. (1986), "Development of micro-concrete for scale model testing of buried structures", Technical Report ESL-TR-85-49, Department of Civil Engineering, University of Florida, Gainesville, Florida.

Dancygier, A.N. and Karinski, Y.S. (1999), "A simple model to assess the effect of soil shear resistance on the response of soil-buried structures under dynamic loads", *Engineering Structures*, **21**(12), December, 1055-1065.

Drake, J.L., Walker, R.E. and Slawson, T. (1989), "Backfill effect on buried structure response", *Proc. of the Fourth International Symposium on the Interaction of Non-Nuclear Munitions with Structures*, **2**, Panama City Beach, Florida, April.

Getchell, J.V., Kiger, S.A., Slawson, T.R. and Hyde, D.W. (1984), "Vulnerability of shallow-buried flat-roof structures", Technical Report SL-80-7, U.S. Army Engineers Waterways Experiment Station, Vicksburg, Missouri.

Keer, L.M., Shah, S.P. and Dancygier, A.N. (1991), "Dynamic response of embedded structures", Technical Report AFOSR-TR-91-0674, AD-A239 019/3/XAB, Department of Civil Engineering, Northwestern University, Evanston, Illinois.

Kiger, S.A., Eagles, P.S. and Baylot, J.T. (1984), "Response of earth-covered slabs in clay and sand backfills", Technical Report SL-84-18, AD-A149296, Waterways Experiment Station, Structures Laboratory, Vicksburg, Miss., October.

Kiger, S.A. (1988), "Ultimate capacity of earth-covered slabs", *ASCE, Journal of Structural Engineering*, **114**(10), October.

Murtha, R.N. (1973), "Arching in soils with cohesion and intergranular friction", Technical Report R-793, AD-766100, NCEL, Port Hueneme, California, July.

Newmark, N.M. (1964), "The basis of current criteria for the design of underground protective construction", *Proc. of the Symposium on Soil-Structure Interaction*, Tucson, Arizona, September.

Weidlinger, P. and Hinman, E. (1988), "Analysis of underground protective structures", *ASCE, Journal of Structural Engineering*, **114**(7), July.

Weidlinger, P. and Hinman, E. (1990), "Cavitation in solid medium", *ASCE, Journal of Engineering Mechanics*, **117**(1), January.

Terzaghi, K. (1943), *Theoretical Soil Mechanics*, John Wiley & Sons, Inc., New York.

Notations

B = width of a rectangular roof
c = pressure wave propagation speed in the soil
c_1 = non-dimensional pressure wave propagation speed in the soil ($c_1^2 = E/M$)
D = depth of burial
E = soil Young's modulus
k = soil arching coefficient
$\tilde{k}$ =non-dimensional arching coefficient ($\tilde{k} = 2k/\rho r$)
L = length of a rectangular roof
M = SDOF (structure) mass per unit area
p_o = external impact amplitude
$p_{\max}$ = peak interface pressure
$p(t)$ = external (surface) load
r, R = radius of the structure roof in the current model
r_{eq} = equivalent structure radius
t = instant time
t_0 = last gap open/closure time ("previous state")
t_G = gap opening time
$T_n(t)$ = function of time, only in the Fourier series
T_0 = external load impulse duration
$U(t, x)$ = vertical soil displacement
$\tilde{\boldsymbol{U}}(\boldsymbol{t},\boldsymbol{x})$ = transformed vertical soil displacement
U_p = soil displacement of the "previous state" (at the time prior to the gap closure of opening)
$\dot{\boldsymbol{U}}_{\boldsymbol{p}}$ = soil velocity of the "previous state"
$\tilde{\boldsymbol{U}}_p(t_0, x)$ = Fourier transformation of the solution of the "previous state" at $t = t_0$
$W(t)$ = SDOF (structure) mass deflection
W_p = mass (structure) displacement
$\dot{W}_p$ = mass (structure) velocity
x = depth corrdinate
$X_n(x)$ = solution's eigenfunction
$\|X_n\|$ = eigenfunction's norm
ϑ_n = solution's eigenvalue
λ_n = normalized system's frequency [$\lambda_n = -(\tilde{k} + c^2\vartheta_n^2)$]
μ = SDOF (structure) spring stiffness per unit area
$\tilde{\mu}$ = non-dimensional spring stiffness ($\tilde{\mu}=\mu/M$)
ρ = soil mass density
$\sigma(t, D)$ = contact (interface) stress between the soil and the structure
$\tau(t, x)$ =friciton traction on the perimeter of the soil column in the current model